

# Rothamsted Repository Download

## A - Papers appearing in refereed journals

Willcock, S., Cooper, G. S., Addy, J. and Dearing, J. A. 2023. Earlier collapse of Anthropocene ecosystems driven by multiple faster and noisier drivers. *Nature Sustainability*. <https://doi.org/10.1038/s41893-023-01157-x>

The publisher's version can be accessed at:

- <https://doi.org/10.1038/s41893-023-01157-x>

The output can be accessed at: <https://repository.rothamsted.ac.uk/item/98wy0/earlier-collapse-of-anthropocene-ecosystems-driven-by-multiple-faster-and-noisier-drivers>.

© 22 June 2023, Please contact [library@rothamsted.ac.uk](mailto:library@rothamsted.ac.uk) for copyright queries.

1 **Title:** Earlier collapse of Anthropocene ecosystems driven by multiple faster and noisier drivers

2  
3 **Author list:** Simon Willcock<sup>1,2\*</sup>, Gregory S. Cooper<sup>3,4</sup>, John Addy<sup>5</sup> and John A. Dearing<sup>6</sup>.

4 **Affiliations:**

- 5 1. Net Zero and Resilient Farming, Rothamsted Research, Harpenden, Hertfordshire, AL5 2JQ,  
6 UK. [simon.willcock@rothamsted.ac.uk](mailto:simon.willcock@rothamsted.ac.uk)
- 7 2. School of Natural Sciences, Bangor University, Bangor, Gwynedd, LL57 2DG, UK.
- 8 3. Institute for Sustainable Food, University of Sheffield, Western Bank, Sheffield, S10 2TN, UK.
- 9 4. Department of Geography, University of Sheffield, Western Bank, Sheffield, S10 2TN, UK.  
10 [g.s.cooper@sheffield.ac.uk](mailto:g.s.cooper@sheffield.ac.uk)
- 11 5. Intelligent Data Ecosystems, Rothamsted Research, Harpenden, Hertfordshire, AL5 2JQ UK.  
12 [john.addy@rothamsted.ac.uk](mailto:john.addy@rothamsted.ac.uk)
- 13 6. Geography and Environmental Science, University of Southampton, Southampton, SO17 1BJ,  
14 UK. [j.dearing@soton.ac.uk](mailto:j.dearing@soton.ac.uk)

15 \* Corresponding author

16  
17 **Abstract**

18 A major concern for the world's ecosystems is the possibility of collapse, where landscapes and the  
19 societies they support change abruptly. Accelerating stress levels, increasing frequencies of extreme  
20 events, and strengthening inter-system connections suggest that conventional modelling approaches  
21 based on incremental changes in a single stress may provide poor estimates of the impact of climate  
22 and human activities on ecosystems. We conduct experiments on four models that simulate abrupt  
23 changes in the Chilika lagoon fishery, the Easter Island community, forest dieback and lake water  
24 quality – representing ecosystems with a range of anthropogenic interactions. Collapses occur sooner  
25 under increasing levels of primary stress, but additional stresses and/or the inclusion of noise in all  
26 four models bring the collapses substantially closer to today by ~38-81%. We discuss the implications  
27 for further research and the need for humanity to be vigilant for signs that ecosystems are degrading  
28 even more rapidly than previously thought.

29  
30 **Key words:** climate change, modelling, regime shift, resilience, stress, tipping point.

31  
32 **Main text:**

33  
34 For many observers, UK Chief Scientist's John Beddington's argument that the world faced a 'Perfect  
35 Storm' of global events by 2030<sup>1</sup> has now become a prescient warning. Recent mention of 'ghastly  
36 futures'<sup>2</sup>, 'widespread ecosystem collapse'<sup>3</sup>, and 'domino effects on sustainability goals'<sup>4</sup> tap into a  
37 growing consensus within some scientific communities that the Earth is rapidly destabilising through  
38 'cascades of collapse'<sup>5</sup>. Kareiva and Carranza<sup>6</sup> even speculate on 'end-of-world' scenarios involving  
39 transgressing planetary boundaries (climate, freshwater and ocean acidification), accelerating  
40 reinforcing (i.e. positive) feedback mechanisms and multiplicative stresses. Prudent risk management  
41 clearly requires consideration of the factors that may lead to these bad-to-worst-case scenarios<sup>7</sup>. Put  
42 simply, the choices we make about ecosystems and landscape management can accelerate change  
43 unexpectedly.

44  
45 The potential for rapid destabilisation of Earth's ecosystems is, in part, supported by observational  
46 evidence for increasing rates of change in key drivers and interactions between systems at the global  
47 scale (SI-1). For example, despite decreases in global birth rates and increases in renewable energy  
48 generation, the general trends of population, greenhouse gas concentrations and economic drivers  
49 (such as gross domestic product) are upwards<sup>8,9</sup> – often with acceleration through the 20<sup>th</sup> and 21<sup>st</sup>  
50 centuries. Similar non-stationary trends for ecosystem degradation<sup>10</sup> imply that unstable sub-systems  
51 are common. Furthermore, there is strong evidence globally for the increased frequency and  
52 magnitude of erratic events, such as heatwaves and precipitation extremes<sup>11</sup>. Examples include the

53 sequence of European summer droughts since 2015<sup>12</sup>, fire-promoting phases of the tropical Pacific  
54 and Indian ocean variability<sup>13</sup>, and regional flooding<sup>11</sup>, already implicated in reduced crop yields<sup>14</sup>, and  
55 increased fatalities and normalised financial costs<sup>9</sup>.

56

57 The increased frequency and magnitude of erratic events is expected to continue throughout the  
58 twenty-first century. The IPCC AR6 concludes that “multiple climate hazards will occur simultaneously,  
59 and multiple climatic and non-climatic risks will interact, resulting in compounding overall risk and  
60 risks cascading across sectors and regions”<sup>11</sup>. Overall, global warming will increase the frequency of  
61 unprecedented extreme events<sup>11</sup>, raise the probability of compound events<sup>15</sup>, and ultimately could  
62 combine to make multiple system failures more likely<sup>16</sup>. For example, there is a risk that multiple  
63 tipping points can be triggered within the Paris Agreement range of 1.5 to 2°C warming, including  
64 collapse of the Greenland and West Antarctic ice sheets, die-off of low-latitude coral reefs, and  
65 widespread abrupt permafrost thaw<sup>17</sup>. These tipping points are contentious and with low likelihood  
66 in absolute terms, but with potentially large impacts should they occur. In evaluating models of real  
67 world systems, we therefore need to be careful that we capture complex feedback networks and the  
68 effects of multiple drivers of change that may act either antagonistically or synergistically<sup>18–20</sup>.  
69 Prompted by these ideas and findings, we use computer simulation models based on four real-world  
70 ecosystems to explore how the impacts of multiple growing stresses from human activities, global  
71 warming and more interactions between systems could shorten the time left before some of the  
72 world’s ecosystems may collapse.

73

74 Intuitively, stronger interactions between systems may be expected to increase the numbers of drivers  
75 of any one system, change driver behaviour and generate more system noise. As a result, we would  
76 anticipate that higher levels of stress, more drivers and noise may bring forward threshold-dependent  
77 changes more quickly. For example, for any particular system (e.g. the Amazon forest) it is possible to  
78 envisage a time sequence that starts with one main driver (e.g. deforestation), then multiple drivers  
79 (e.g. deforestation plus global warming), more noise through extreme events (e.g. more droughts and  
80 wildfires), with additional feedback mechanisms that enhance the drivers (e.g. diminished internal  
81 water cycle and more severe droughts). A vortex could therefore emerge, with drivers generating  
82 noisier systems as climate variability and the incidence of extreme events increases. Under worst-case  
83 scenarios, the circle becomes faster as reinforcing feedbacks accelerate connections or human  
84 activities increase stress levels. However, extreme events could also counteract each other (e.g.  
85 extreme droughts and extreme rainfall events) and interconnections could also have weakening  
86 effects – for example where increased plant growth driven by increased CO<sub>2</sub> is counterbalanced by  
87 increased temperatures and droughts. To date, there is limited observational evidence showing that  
88 ecosystems have a record of tipping between alternate stable states<sup>21</sup>.

89

90 Ashwin *et al.*'s<sup>19</sup> mathematical tripartite classification of critical transitions includes slow driver  
91 bifurcations, rate-induced (fast/cumulative driver) and noise-induced (extreme event) tipping points.  
92 However, previous studies tend to focus on each of these categories individually. For example, there  
93 is a well-established body of physics and mathematical theory on ‘mean exit times’<sup>22</sup>, with studies  
94 investigating the timing of tipping points in rate-induced<sup>18–20</sup> or noisy<sup>19,23,24</sup> systems. However, despite  
95 calls for more experimental evidence of the impacts of climate variability and extremes on  
96 ecosystems<sup>25,26</sup>, the relative importance or combined effect of fast drivers, multiple drivers and noisy  
97 system drivers on the collapse of real world ecosystems is not known. Critical transitions driven by  
98 current pollution forcings such as greenhouse gas emissions<sup>27</sup> and nutrient loadings<sup>28</sup> are likely to be  
99 novel, well beyond the envelope of natural variability. Hence, we avoid the use of the terms critical  
100 transition and tipping points, used formally in dynamical systems theory to represent shifts to  
101 alternative attractors, and focus on abrupt threshold-dependent changes (ATDCs) that would be  
102 perceived by society as the quantitative (e.g. fish stock integrity) and/or qualitative (e.g. ecosystem  
103 functions) collapse of a desirable system state<sup>29,30</sup>.

104

105 We have selected a range of system dynamic models that have been previously used to demonstrate  
106 generalisable findings (e.g. with regard to safely overshooting ATDCs<sup>27</sup>) and can be externally  
107 manipulated to simulate internal emergent ATDCs at local and regional scales – as if they were  
108 impacted through stronger connections to other systems. Reflecting modern ecosystems, these  
109 models show varied anthropogenic interactions, ranging from social-ecological systems with strongly  
110 coupled human-nature feedbacks to ecological systems with predominantly one-way interactions  
111 where ecosystems are influenced by the external impacts of people. The ability of these models to  
112 capture feedback-loops, delays and interactions between components is well established<sup>31,32</sup>, and has  
113 motivated their use in various recent studies of sustainability and resilience<sup>21,33–35</sup>. Therefore, guided  
114 by Ashwin *et al.*'s<sup>19</sup> typology of tipping points, we aim to generalise the dynamics of increasing the  
115 numbers of drivers, their rates and variability (as proxies for stronger interactions between systems  
116 and noise) on the speed at which ATDCs are reached in four ecosystem dynamics models (Figure 1):  
117 Lake Chilika lagoon fishery<sup>21,33</sup>, Easter Island<sup>36</sup>, Lake phosphorus<sup>28,37</sup>, and a modified version of The  
118 Hadley Centre Dynamic Global Vegetation Model (TRIFFID) of forest dieback<sup>27,38</sup>.

119

## 120 **Results**

121 As described in the Methods, the four models each have a primary (baseline) slow driver (Figure 2:  
122 grey boxplots), where linear changes in their trajectories over time can initiate ATDCs in their  
123 respective outcome variable (Lake Chilika: fish population; Easter Island: human population; TRIFFID:  
124 tree coverage; Lake phosphorus: lake phosphorus concentration). When the strength of the primary  
125 slow driver in each model is increased, the modelled systems collapse sooner - as defined by a  
126 statistical breakpoint in their temporal trends (see Methods Section 3.2). Increasing the strength of  
127 multiple drivers with additional secondary and tertiary drivers further reduces the breakpoint date  
128 (Figure 2), with variation around these median responses determined by the relative strength of the  
129 additional drivers – with addition of a weak secondary driver bringing forward the start of system  
130 collapse substantially less than the addition of a strong secondary driver (Figure S2-1).

131

132 In addition to earlier breakpoint dates, extra drivers can also cause ATDCs at levels where it would be  
133 resilient to the primary slow driver in isolation (SI-2). For example, across the 1000 timesteps of the  
134 Lake phosphorus model, the system is stable at normalised baseline driver rates up to 0.348 (i.e., Lake  
135 phosphorus concentration does not go through a breakpoint; Figure S2-4D). However, the addition of  
136 a single secondary driver of normalised strength 0.3 can lead to breakpoints occurring at normalised  
137 primary driver strengths 0.312 (reduction from baseline: 0.036 [10.3%]; Figure S2-4D), and the  
138 addition of an extra tertiary driver with normalised strength 0.3 can lead to breakpoints at normalised  
139 primary strengths 0.270 (reduction from baseline: 0.078 [22.4%]; Figure S2-4D). With all additional  
140 drivers, 12.3% of breakpoints observed in the Lake phosphorus model occurred at primary driver  
141 strengths below the minimum threshold required to result in a breakpoint when the primary driver is  
142 acting in isolation (Lake Chilika: 1.2%; Easter Island: 14.8%; TRIFFID: 7.7%; Table S2-1).

143

144 Next, for each of the four models, the trajectories of the primary slow drivers were randomly  
145 perturbed by the addition of noise (Methods Section 2.3). Noise was generated within the system  
146 dynamics software used to run the models (STELLA<sup>39</sup>) by randomly sampling per timestep from a  
147 normal distribution with a mean value of 0 and standard deviation of  $\sigma$  (sigma), meaning that random  
148 perturbations on the system could work in both positive ( $\sigma > 0$ ) and negative directions ( $\sigma < 0$ ). The  
149 value of  $\sigma$  was randomly sampled once per simulation to explore the effects of different noise scales  
150 on the time to reach the breakpoint date (Methods Section 2.3). The addition of high noise  
151 (normalised  $\sigma$  values  $> 0.666$ ) shows that increasing the variability of the primary slow driver (in  
152 isolation) across all four models can bring forward the date of system collapse (Figure 3).

153

154 The effects outlined above are synergistic – combining multiple drivers with noise further reduces the  
155 breakpoint date beyond the effects of either multiple drivers or noise acting alone (Figure 4). For  
156 example, at a normalised slow baseline driver strength of 0.3 in the Easter Island model (Figure 4B),  
157 the addition of low uncoupled noise (normalised  $\sigma$  values  $\leq 0.333$ ) with all possible additional drivers  
158 switched on with normalised strengths of over 0.666 (i.e. ‘high’ secondary and tertiary trajectories)  
159 brings the median breakpoint forward from timestep 1179 to timestep 426 (63.8% reduction),  
160 whereas high noise levels (defined as normalised  $\sigma$  values  $> 0.666$ ) brings the breakpoint forward from  
161 timestep 1179 to timestep 225 (80.9% reduction). The finding that the breakpoint date is most  
162 advanced by the combination of high noise and high secondary trajectories is consistent across the  
163 other three models, with the median breakpoint date at a normalised slow baseline driver strength of  
164 0.3 changing from year 2047 to year 2035 (37.5% reduction) for Lake Chilika, timestep 238 to timestep  
165 92 (61.3% reduction) for TRIFFID, and timestep 848 to timestep 388 (54.2% reduction) for Lake  
166 phosphorus. Across all combinations of noise and multiple drivers, 1.7%, 7.5%, 6.6% and 8.9% of  
167 modelled breakpoints occurred at primary driver strengths below the minimum threshold required to  
168 result in a breakpoint when acting in isolation for Lake Chilika, Easter Island, TRIFFID and Lake  
169 phosphorus respectively (Table S2-4).

170

171 All results presented above are robust to different modelling and monitoring decisions. For example,  
172 these results are consistent regardless of whether the noise is coupled to (i.e. allowed to grow with)  
173 the magnitude of the primary slow driver or uncoupled and sampled from a constant distribution  
174 (Figure S2-2 & S2-3; Table S2-3 to S2-5), and irrespective of whether linear, non-linear or threshold-  
175 type boundaries<sup>40</sup> are used to define the breakpoints (SI-4; Figures S4-1 to S4-6).

176

## 177 Discussion

178 Previous findings have supported the idea that Earth’s subsystems may interact to the extent that an  
179 abrupt shift in one raises the probability that a shift may occur in another<sup>41–43</sup>. In this paper we  
180 have explored through four ecosystem models how these interactions may alter the timing of ATDCs  
181 through the effects of strengthened drivers, multiple drivers and higher internal variability or  
182 noise. The potential effects are substantial with combinations of a strengthened main driver, an  
183 additional driver and noise giving at least 38-81% reductions in the future date of a predicted ATDC  
184 compared to estimates for a non-interacting system with a constant single driver and no  
185 noise. Importantly, the effect per unit time on bringing forward an ATDC is greatest at low driver  
186 trajectories, which further strengthens the suggestion that abrupt Earth system changes may occur  
187 sooner than we think (SI-1). Our findings also show that 1.2-14.8% of ATDCs can be triggered by  
188 additional drivers and/or noise below the threshold of driver strengths required to collapse the system  
189 if only a single driver were in effect.

190

191 Overall, we find that as the strength of a main driver increases, the systems collapse sooner. Adding  
192 multiple drivers brings collapses further forward, as does adding noise, and the two effects can be  
193 synergistic. However, the relative importance of these changes varies across systems. For the Chilika  
194 fishery, the most influential driver is captured as the primary driver and so additional drivers have  
195 limited influence, with the addition of noise in the primary driver bringing the breakpoint date much  
196 closer to the present. For Easter Island, TRIFFID, and Lake phosphorus, the opposite is true – the  
197 addition of high levels of noise in the primary driver advances the date of system collapse far less than  
198 additional drivers. Thus, while the earliest collapses in all the systems are found when both additional  
199 drivers and noise are applied, an important implication for real world governance is that the precise  
200 importance of individual driver trajectories and noise is system-dependent.

201

## 202 Earlier occurrence of abrupt threshold-dependent changes

203 Our results show that systems do not collapse at a constant level of cumulative stress (i.e., total stress  
204 built up over time) irrespective of the rate of stress change (SI-5) but rather underline the importance  
205 of rate over accumulated stress<sup>18–20</sup>. Simulations where the primary, secondary or tertiary drivers

206 change more rapidly tend to shift earlier and are less able to absorb cumulative stress (Figure SI5-1).  
207 Thus, the same ecosystem can collapse as a result of sustained/cumulative pressure of a slower driver,  
208 but will likely collapse faster if the rate of change is increased<sup>18–20</sup>. Increasingly fast driver rates will  
209 eventually overwhelm the ability of balancing feedback loops to compensate for increased stress on  
210 the system; thus, signifying a loss of resilience. In the absence of strong balancing loops, a fast driver  
211 allows reinforcing feedback loops to grow (SI-6). The driver may also re-energise dormant reinforcing  
212 feedback loops or allow new coupled, reinforcing feedback mechanisms to emerge (cf. <sup>44</sup>). For the  
213 Easter Island, TRIFFID and Lake phosphorus models, as the balance of feedback loops shifts towards  
214 reinforcing loops, the probability that the system will be driven out of its attractor into an ATDC  
215 increases (SI-6). Additional drivers limit further the balancing ability of balancing feedback loops and  
216 increase the probability of collapse. For Lake Chilika, the pre-ATDC phase is dominated by reinforcing  
217 feedback loops driving fisher population growth towards dangerous levels, with collapse coinciding  
218 with the growth of balancing feedbacks in the form of reduced fish populations. These rebalance the  
219 system by limiting the effectiveness of the fisher population's fishing efforts (Figure S6-1).

220

221 In our analysis, the rise in driver stress is continuous over time. Where the stress is applied in discrete  
222 events, for example, wildfire events, the same response can be expected where elapsed time between  
223 events is insufficient for balancing feedback loops to rebalance the system or where significantly large  
224 stress events motivate additional amplifying loops. This is similar to the impact of extreme events (i.e.,  
225 noise, Figures 3 and 4), which has the ability to push a system out of its attractor temporarily or  
226 permanently; an effect that strengthens as the system becomes increasingly sensitive to perturbations  
227 close to a potential ATDCs<sup>19,23</sup>. However, sequences of extreme events from multiple drivers, such as  
228 extreme drought followed by extreme rainfall, may only act antagonistically where sufficient time  
229 allows for the system to repair the extreme impacts. Our study only looks at driver noise; there could  
230 coincidentally or equally be natural 'state' change/noise (vertical axis on phase-plot figures) – for  
231 example, natural tree mortality, natural lake infilling, fluctuating populations in ecosystems, or ageing  
232 population, behavioural/psychological changes in the social domain – all of which could alter the  
233 probability of ATDCs even in the absence of, or changes in, the external drivers<sup>19,23</sup>.

234

### 235 Moving forward

236 These results have research implications for further developing and applying models of ecosystems to  
237 study ATDCs. Whilst our findings derive from models based on real-world systems, the greater  
238 complexity of reality may limit the transferability of our results. The Lake Chilika model is the most  
239 complex of the four models, with upwards of 100 model variables capturing hydroclimatic,  
240 ecohydrological, fishery and socio-economic dynamics interacting to create four balancing loops and  
241 seven reinforcing loops – and is validated against historical data<sup>33</sup>. Of all the models, it shows the least  
242 dramatic reductions in the date of any ATDC (SI-1). Therefore, it is plausible that more complex  
243 systems will have stronger regulating mechanisms that stabilise the system through sets of balancing  
244 feedback loops<sup>44</sup>, constraining the more extreme of our findings.

245

246 Mechanistically, in simpler models, such as the Lake phosphorus model, regime shifts may be  
247 triggered by a single feedback loop. In more complex models (and likely ecosystems), our analysis of  
248 feedback strengths shows evidence for an instability cascade through the system via multiple  
249 feedback loops. For example, the collapse in the Easter Island human population reflects the  
250 cumulative effects of several feedback loops triggered by over-harvesting the tree population.  
251 Growing instability weakens the balancing feedbacks for the tree population, rat population and  
252 agricultural carrying capacity (Figure S6-2), allowing the reinforcing loop for the decline in human  
253 population to strengthen. In general, increasing driver strengths can trigger these mechanisms earlier,  
254 whereas additional drivers have the ability to shift the nature of the cascade (e.g. including/excluding  
255 different feedbacks; Figures S6-5 to S6-8). However, in spatial terms, multiple interacting feedback  
256 mechanisms may lead to spatial re-organisation which slows the rate of collapse<sup>45,46</sup>, with stochasticity

257 promoting temporal stability – particularly in local regions with small populations<sup>24</sup>. There is the  
258 possibility, too, that interconnections could have weakening effects and, where the impacts are slower  
259 than the system response, extreme events could counteract each other. Thus, our quantitative  
260 findings could be viewed as representing worst-case scenarios for the different ecosystems<sup>7</sup>.

261

262 Nevertheless, the finding that additional stress produces qualitatively similar emergent phenomena  
263 in a range of simulation models should not be dismissed lightly<sup>47,48</sup>. The consistency across models  
264 representing varying processes, interactions and contexts may indicate that equifinality makes the  
265 accurate representation of internal system dynamics less important than the external drivers/stresses  
266 in simulating complex realities<sup>49</sup>. Clearly, model development is required to better capture the  
267 diversity of system elements, interactions, and feedbacks for more complex systems, and in particular,  
268 more realistic coupling of human decision making and ecological/environmental dynamics. With the  
269 exception of Lake Chilika<sup>33</sup>, each model in this study was originally created to study the impact of a  
270 primary driver influenced by predominantly external anthropogenic processes, presumably the driver  
271 perceived as the most impactful. Our results show that this assumption may not be the case (e.g.  
272 Easter Island) and models should include a range of plausible drivers and scenario combinations if they  
273 are to avoid underestimating the risk of ATDCs. Moreover, new ecosystem models should allow for  
274 the growth of feedback loops and long-term simulations in order to observe the mechanisms that  
275 underpin ATDCs<sup>48,50</sup>. For example, more realistic social-ecological coupling may lead to shifts in the  
276 human decisions capable of either shifting an ATDC much closer to the present or avoiding it  
277 completely. Monitoring of real-world systems should therefore capture multiple plausible drivers,  
278 their variability, and their feedbacks to social systems. More ATDCs will occur unexpectedly if the focus  
279 on perceived main drivers ignores other drivers that increase cumulative stress and gradually reduce  
280 the resilience of systems, as exemplified in the lake water regime shift at Erhai, western China<sup>28</sup>. There,  
281 abrupt lake eutrophication was initially perceived to have been driven by transgression of a threshold  
282 in nutrient enrichment driven by agricultural runoff, but historical analysis has shown that the shift  
283 was also affected by lake water level management, seasonal climate and fish farming<sup>44</sup>.

284

285 Significant research has focused on identifying early warning metrics linked to critical slowing down  
286 theory which applies primarily to ‘equilibrium’ system states with single, slow drivers<sup>51</sup>. If, as we  
287 indicate, real world tipping elements are more likely to be driven by multiple, fast drivers and extreme  
288 events, it is less likely that early warning signals in the frequency domain will be observed<sup>20,51</sup> for noise-  
289 induced thresholds. Certainly, excluding noise from model systems, whilst a potentially useful  
290 simplification for theoretical understanding, risks creating a false sense of security by overestimating  
291 the distance remaining before critical thresholds are breached in the real world where multiple drivers  
292 and noise are abundant<sup>27,52</sup>. Therefore, alternative approaches to identifying resilience loss in real  
293 systems prior to ATDCs through structural metrics<sup>53–55</sup> and early warning signals generated by agent-  
294 based models<sup>50</sup> should be considered more widely.

295

296 Previous studies of interactions between tipping elements have focused on large scale systems and  
297 suggest significant social and economic costs from the second half of the 21st century onwards<sup>42,56</sup>.  
298 Our findings suggest the potential for these costs to occur sooner. For example, it is not clear whether  
299 the IPCC’s estimate for a tipping point in the Amazon forest prior to 2100<sup>11</sup> includes the possibility for  
300 interacting drivers and/or noise; if not, our findings suggest a breakdown may occur several decades  
301 earlier (SI-1). This would occur where local scale failures in elements (such as species populations, fish  
302 stocks, crop yields and water resources) combine with more extreme events (such as wildfires and  
303 droughts) to precondition the large-scale system, already vulnerable to the influence of other large-  
304 scale tipping elements, to collapse earlier – a meeting of top-down and bottom-up forces (SI-1). This  
305 vertical integration of forces is reinforced by the rising trend in global warming that already represents  
306 a spatial integrator which may be expected to strengthen before it subsides. Clearly, climate  
307 economics need to incorporate these synergistic and cumulative effects that are occurring at local and

308 regional scales into larger scale models where they are currently lacking<sup>57,58</sup>. The dominance of  
309 accelerating trends in global time-series of economic consumption [e.g.<sup>9,59</sup>] makes our finding that  
310 ramping up the main driver is the easiest way to bring forward an ATDC particularly worrying. Similarly,  
311 the implication for regions experiencing more extreme events is that an ATDC may occur even before  
312 the main driver has ramped up.

313

314 The commonality of findings across four well-studied ecosystems has potentially profound  
315 implications for our perception of future risks associated with the climate and ecological crises. While  
316 it is not currently possible to predict how climate-induced ATDCs and the effects of local human  
317 actions on ecosystems connect across temporal and spatial scales, our findings show the potential for  
318 each to reinforce the other. The ability of present policy and practice to prevent an ever-deepening  
319 vortex of degradation in local and regional ecosystems requires urgent investigation<sup>7</sup>.

320

## 321 **Methods**

322

### 323 1. Overview of systems models

324 Here we briefly describe the four previously published models used to investigate the effects of  
325 multiple drivers and noise upon the timing of ATDCs. Each model was replicated and simulated within  
326 the system dynamics software STELLA Architect v.1.6.1<sup>39</sup>, with outputs exported into CSV files as time  
327 series and analysed in the statistical software R v.4.1.0<sup>60</sup>. The models, example data and code used in  
328 the analyses are available via: <https://doi.org/10.5281/zenodo.7946433>.

329

330 The **Lake Chilika fishery** model<sup>21,33</sup> is a social-ecological model designed to simulate the future fish  
331 population and catch trajectories of the Chilika lagoon, Odisha, India. The model is able to explore the  
332 impacts of multiple slower drivers (i.e., fisher population growth and increased rainfall and  
333 temperatures under climate change) and multiple faster drivers (i.e. abrupt changes in fish prices and  
334 fishing gear) on the sustainability and resilience of the fish population until 2100. As described in detail  
335 in <sup>33</sup>, the model includes coupling between multiple social and ecological components of the system.  
336 First, the efficiency of fish catch efforts is proportional to the fish population density within the lagoon  
337 (i.e. as fish density declines, catch per unit effort also decreases). Second, as a form of environmental  
338 carrying capacity, the fisher population growth is proportional to the total number of livelihoods  
339 supportable by the overall fishery value, which is derived from the total fish catch in any given month.  
340 Third, fishers may invest their fishing revenues into more intensive fishing gear (i.e. motorboats),  
341 which also has implications for fish catch and fish stock health over time. The model is also able to  
342 simulate multiple natural resource governance approaches (e.g. fishing quotas and alternative  
343 livelihoods), although the model runs conducted here are all under the baseline governance scenario<sup>33</sup>  
344 (i.e. the tidal outlet between the lagoon and the Bay of Bengal is reopened every ten years to  
345 rejuvenate fish migration and lagoon salinity). The model has been previously validated against  
346 empirical data through standard behaviour matching techniques and Monte Carlo sensitivity  
347 analysis<sup>33</sup>. The Lake Chilika model is run for a total of 1536 timesteps (months), with each timeseries  
348 aggregated to the annual scale (c.1973-2100). Future trajectories, detailed in Method Sections 2.2-  
349 2.4, activate from timestep 504 (i.e. January 2015) after the completion of the historical  
350 parameterisation and validation periods<sup>33</sup>.

351

352 The **Easter Island** model aims to explore alternative hypotheses behind the collapse of the Easter  
353 Island civilisation<sup>36</sup>. The initial parameterisation of the model here is the same as the 'ecocide'  
354 configuration detailed in <sup>36</sup>. The main internal social-ecological feedback driving model dynamics is  
355 the balancing feedback between human population growth, tree coverage and land clearance,  
356 whereby the overharvesting of the primary resource (palm forest) can lead to overshoot dynamics  
357 and the eventual demise of the human population (i.e. 'ecocide'). As noted in <sup>36</sup> (p.1): "*While it is*  
358 *obvious that the islanders were not directly living from palm trees, the forest provided several valuable*



359 and difficult to substitute ecological services, including food from fruits and palm nuts, timber to  
 360 construct houses and sea-going canoes for fishing". In addition to this main internal social-ecological  
 361 feedback, multiple external variables can be modified to change the speed of human population  
 362 growth, including the tree clearance rate per capita, the maximum carrying capacity of the agricultural  
 363 system (i.e. to help support human population growth), and the mortality rate of trees (i.e.  
 364 representative of potential disease outbreaks). The model is run for 1500 timesteps (years), with  
 365 future scenarios active from the first timestep (Method Sections 2.2-2.4).

366  
 367 The **TRIFFID** model is a modified version of The Hadley Centre Dynamic Global Vegetation Model,  
 368 originally developed by Cox *et al.*<sup>38</sup> to explore the effects of atmospheric CO<sub>2</sub> concentrations on the  
 369 rate of Amazon dieback. Here we simulate the modified version developed by Ritchie *et al.*<sup>27</sup>, which is  
 370 based around a central Lotka-Volterra equation describing the change in vegetation coverage as the  
 371 primary external driver (local atmospheric temperatures) increases. On any given timestep, the  
 372 change in vegetation coverage ( $dv/dt$ ) is driven by a temperature dependent growth term and an  
 373 externally set disturbance rate:

$$374 \quad \frac{dv}{dt} = gv(1 - v) - yv \quad (\text{Equation 1a})$$

$$375 \quad g = g_0 \left[ 1 - \left( \frac{T_i - T_{opt}}{\beta} \right)^2 \right] \quad (\text{Equation 1b})$$

$$376 \quad T_l = T_f + (1 - v)\alpha \quad (\text{Equation 1c})$$

377 Where  $v$  is the vegetation coverage,  $T_f$  is the temperature forcing parameter (Methods Section 2.3),  $g$   
 378 is the vegetation growth rate,  $g_0$  is the maximum growth rate (2/year),  $y$  is the disturbance rate  
 379 (Methods Section 2.4),  $T_l$  is the local temperature,  $T_{opt}$  is the optimal temperature (28°C),  $\beta$  is the half-  
 380 width of the growth versus temperature curve (10°C) and  $\alpha$  is the difference in temperature between  
 381 surface bare soil and forest (5°C). Therefore, the growth term is assumed to be parabolic with the local  
 382 temperature (Equation 1b), meaning that once the local temperature increases beyond the optimal  
 383 temperature, negative tree growth ensues [i.e. additional tree mortality<sup>27</sup>], which in turn leads to an  
 384 increase in temperature (Equation 1c), which may eventually produce the runaway loss in tree  
 385 coverage. Although the meaning of the disturbance rate is not specified by Ritchie *et al.*<sup>27</sup>, it may proxy  
 386 human-induced ecosystem stresses such as deforestation for agricultural land and disease-driven  
 387 forest dieback. The model is run for 500 timesteps, with future trajectories active from the first  
 388 timestep (Method Sections 2.2-2.4).

389  
 390 The **Lake phosphorus** model is a simplified version of the original 'lake response to P input and  
 391 recycling' model<sup>37</sup>, as modified by Wang *et al.*<sup>28</sup>. The model is designed as a simple ecosystem model,  
 392 with lake water phosphorus concentration driven by a generic external phosphorus input (which may,  
 393 for example, proxy external inputs from agricultural runoff, sewage, and industrial discharges from  
 394 factories, construction sites, and urban areas)<sup>61</sup>. In turn, lake water phosphorus is recycled back into  
 395 the system as an ecological reinforcing feedback loop, proportional to the lake phosphorus  
 396 concentration on any given timestep. Phosphorus is also removed from lake waters via sedimentation,  
 397 where the volume removed in sediment is proportional to the phosphorus concentration of the lake.  
 398 Therefore, on any given timestep, the change in lake phosphorus concentration ( $dP/dt$ ) equals:

$$399 \quad dP = \left[ a - sP + r \frac{P^n}{P^n + 1^n} \right] dt \quad (\text{Equation 2})$$

400 Where  $P$  is phosphorus concentration,  $a$  is phosphorus input rate (Methods Section 2.3),  $r$  is the  
 401 maximum recycling rate (Methods Section 2.4),  $s$  is the phosphorus loss rate (Methods Section 2.4),  $n$   
 402 is the strength of the recycling response to phosphorus concentrations ( $n = 8$ ) and  $t$  is time. The model  
 403 is run for 1000 timesteps (unitless), with future scenarios active from the first timestep (Method  
 404 Sections 2.2-2.4). Given the simplicity of this model, an area for future research could be expanding  
 405 the original model to explore how adaptive management mechanisms may help to avoid ecosystem  
 406 thresholds, for example, by linking government fertiliser incentives to lake phosphorus levels as the  
 407 ecosystem approaches a threshold.

408

409 2. Generation of future scenarios

410 Using the above models, we performed four *in silico* experiments (presented visually in Figure 1):

- 411 - **Experiment #1:** only the primary slow driver in each model changes over time, and all other
- 412 drivers remain constant (Figure 2 baseline);
- 413 - **Experiment #2:** multiple slow rates, with up to two additional (i.e., 'secondary' and 'tertiary')
- 414 slow trajectories on top of the primary driver changing over time (Figure 2 multiple drivers);
- 415 - **Experiment #3:** the addition of noise to the primary trajectory (Figure 3), with all other drivers
- 416 held constant. The magnitude of noise may be either coupled or uncoupled from the
- 417 trajectory of the primary driver (Methods Section 2.3);
- 418 - **Experiment #4:** the addition of noise to the primary driver, with up to two additional slow
- 419 drivers (Figure 4). The magnitude of noise may be either coupled or uncoupled from the
- 420 trajectory of the primary driver (Methods Section 2.3).

421 In order to survey a wide range of future trajectories (Methods Sections 2.2) and generate a sufficient

422 number of simulations that collapsed (Methods Section 3), each of the models were ran for the

423 following number of iterations (including both 'coupled' and 'uncoupled' settings):

- 424 - Chilika fishery: 70,000
- 425 - Easter Island: 70,000
- 426 - TRIFFID: 70,000
- 427 - Lake phosphorus: 120,000

428 In turn, to maximise computational efficiency both in STELLA and in R, the following logic was applied

429 to the in-built Monte Carlo function in STELLA to automatically generate the four different experiment

430 types described above (the baseline primary driver always remains 'on/active'):

- 431 - IF  $\mu_1 > 0.4$  THEN *Secondary driver active* ELSE *Secondary driver remains at default value*
- 432 - IF  $\mu_2 > 0.4$  THEN *Tertiary driver active* ELSE *Tertiary driver remains at default value*
- 433 - IF  $\mu_3 > 0.4$  THEN *Noise active* ELSE *Noise level remains at zero*

434 Where  $\mu_1, \mu_2$  and  $\mu_3$  represent 'on switches', with values randomly sampled from uniform distributions

435 between 0 and 1 per simulation. The number of simulations per model experiment which showed

436 ATDCs are detailed in Table S3-1.

437

438 Whilst some insights could be obtained deterministically<sup>62</sup>, this is not possible for all models (e.g. Lake

439 Chilika) nor for all experiments (i.e. those involving additional noise). Thus, undertaking these model

440 runs and analyses of the outputs (below) is the most consistent, feasible approach suitable across all

441 models and experiments, allowing for comparisons across experiments, as well as investigation of

442 synergistic impacts – fulfilling our primary aim of investigating the impact of the interaction of fast

443 drivers, multiple drivers and system noise on the timing of tipping points in ecosystems.

444

445 In order to investigate Experiment #1, each of the four models has one primary baseline driver which

446 changes from its default value in every simulation:

- 447 - Lake Chilika fishery: Fisher population growth rate (net difference between the birth rate per
- 448 1000 population and the death rate per 1000 population)
- 449 - Easter Island: Tree clearance rate (trees/person/year)
- 450 - TRIFFID: local temperature (°C)
- 451 - Lake phosphorus: Phosphorus input rate (unitless)

452 Baseline outputs were generated with the Primary driver active AND the Secondary and Tertiary driver

453 remaining at its default value AND the Noise level remaining at zero (Table S3-2). In turn, the Monte

454 Carlo sensitivity analysis function in STELLA randomly samples a future change trajectory for the

455 primary slow driver per simulation (as plotted on the horizontal axes of Figures 2-4). The primary

456 trajectory is sampled between the lower and upper limits of uniform distribution bounds, meaning

457 that there is a uniform likelihood of selecting any given trajectory between the bounds (Table S3-2).

458 A future change trajectory of '0' would cause no change from the default value; the maximum

459 trajectory change limits for each of the models can be seen in Table S3-2.

460

461 The built-in STELLA 'TIME' function generates future scenario trajectories that change linearly over  
462 time (i.e., with a constant gradient over the model horizon). Therefore, the value of the primary driver  
463 at any given timestep equals:

$$464 \quad \text{Scenario value}_{i,t} = \text{TIME}_{i,t} \times \left( \frac{\text{Maximum trajectory value}_i}{\text{Total number of timestep in model}} \right)$$

465 (Equation 3)

466 Where 'i' equals the simulation number and 't' equals the timestep (e.g. t = 1, 2, 3... total number of  
467 timesteps in model). Using the Easter Island model as an example: if a maximum tree clearance value  
468 of 7 has been sampled for the given simulation, then its value after 500 timesteps would be equal to  
469 500 x (7/1500) = 2.333. The plausible trajectory funnels for each of the primary drivers are plotted in  
470 Figure S3-1.

471  
472 To simulate Experiment #2, 'secondary' and 'tertiary' driver trajectories are also activated using the  
473 following logic:

- 474 - 'Secondary': Primary driver active AND Secondary driver active AND Tertiary driver remains  
475 at default value AND Noise level remains at zero OR
- 476 - 'Tertiary': Primary driver active AND Secondary driver remains at default value AND Tertiary  
477 driver active AND Noise level remains at zero OR
- 478 - 'All': Primary driver active AND Secondary driver active AND Tertiary driver active AND Noise  
479 level remains at zero

480 For each model, this specifically involved the following variables (Table S3-2):

- 481 - Lake Chilika fishery: (i) Annual rainfall totals and mean near-surface air temperatures, as per  
482 IPCC (2013) climate change projections for the east coast of India (ii) Price of fish per unit (i.e.  
483 Indian rupee/kg), leading to a more commercially-oriented fishery, with an increasing number  
484 of fishers able to upgrade from traditional fishing boats to more intensive motorboats<sup>33</sup>.
- 485 - Easter Island: (i) Agricultural carrying capacity of the system, which enables a higher human  
486 population to be supported per unit of land cleared for agriculture; (ii) The mortality rate of  
487 trees as a proxy for a disease-spread event.
- 488 - TRIFFID: (i) Temperature-independent disturbance rate of vegetation coverage, i.e., causes of  
489 forest clearance which are not directly linked to temperature changes (e.g. deforestation).  
490 Note: Due to the small size of the model, TRIFFID does not have a tertiary driver.
- 491 - Lake Phosphorus: (i) Rate of phosphorus recycling within the lake environment, (ii) Rate of  
492 phosphorus removal from the lake via sedimentation.

493 For the Lake Chilika and Easter Island models, these additional drivers are external forcings (similar to  
494 the primary driver). However, since the TRIFFID and Lake phosphorus models are designed with only  
495 a single external forcing, additional drivers were also generated internally by altering parameters that  
496 operate on state variables. Whilst mathematically, internal and external forcings are fundamentally  
497 different things, both potentially impact the state of the system and, ecologically, changing internal  
498 model parameters can act as a proxy for an external process causing that change. For example, in the  
499 Lake phosphorus model we have a system with a bifurcation in one dimension of slow external forcing  
500 ( $\alpha$ ) and we additionally vary internal parameters of the system (P recycling rate and P removal rate)  
501 as a proxy for, for example, anthropogenic disturbance impacting the species composition within the  
502 lake<sup>63</sup>.

503  
504 Each of the additional driver trajectories are produced via the same approach as in Equation 3: the  
505 Monte Carlo sensitivity analysis function in STELLA randomly samples a trajectory between the lower  
506 and upper bounds of a uniform distribution for each driver (Table S3-2); in turn, the TIME function  
507 linearly increases the value of the driver from its default value to its sampled trajectory value by the  
508 final timestep of the model horizon.

509  
510 In order to produce one secondary trajectory per simulation in the Lake Chilika model, the sampling  
511 of rainfall and temperature trajectories are connected along a linear gradient, ranging from no change

512 to a combination of +30% rainfall change and +4.5°C temperature change by 2081-2100 relative to  
 513 1986-2005 [as per RCP8.5 projections for the east coast of India<sup>64</sup>]. In STELLA, this is operationalised  
 514 by the model variable ‘climate change trend’, with Monte Carlo sensitivity analysis in STELLA randomly  
 515 sampling a value between 0 and 1 per simulation. As an illustration, if a value of 0.6 was to be sampled,  
 516 then the change in rainfall by 2081-2100 (relative to 1986-2005) would equal 0.6\*30(%) = 18%, whilst  
 517 the change in temperature would equal 0.6\*4.5(°C) = 2.7°C.

518

519 In order to investigate Experiment #3 and Experiment #4, the value of each primary slow driver is  
 520 perturbed per timestep by randomly generated noise. We simulate a standard Wiener process to  
 521 generate noise, equal to  $\sqrt{dt} \times N(0,1)$ , where ‘dt’ equals change in time and ‘N(0,1)’ is a normal  
 522 distribution with a mean of 0 and standard deviation of one. In turn, the product of the Wiener process  
 523 is multiplied by the scaling factor ‘sigma’ ( $\sigma$ ), providing an overall level of noise to be added to the  
 524 value of the primary driver on any given timestep. As per the future trajectories, the magnitude of ‘ $\sigma$ ’  
 525 is randomly sampled once per simulation from uniform distributions, with lower and upper limits  
 526 shown in Table S3-2.

527

528 Therefore, building on Equation 3 above, the value of a primary driver at any point in time in  
 529 Experiment #3 and Experiment #4 equal:

$$530 \quad \text{Scenario value}_{i,t} = \text{TIME}_{i,t} \times \left( \frac{\text{Maximum trajectory value}_i}{\text{Total number of timestep in model}} \right) + (\sigma_i \times \sqrt{dt} \times N(0,1)_t)$$

531 (Equation 4)

532 Equation 4 as detailed above only refers to the ‘uncoupled’ noise simulations. Therefore, to explore  
 533 the effects of ‘coupled’ noise, whereby the magnitude of noise increases with the growth in the  
 534 primary driver, 20,000 simulations were run per model spread evenly between Experiments #3 and  
 535 #4, with the magnitude of noise coupled to the magnitude of the primary driver trajectory. Given the  
 536 differences in the shape of the noise spectrums, we do not directly compare outcomes from the  
 537 uncoupled and coupled noise simulations in this study. Instead, the purpose of modelling coupled  
 538 noise is to ascertain whether worsening magnitudes of extreme events over time are associated with  
 539 earlier ATDCs. In the coupled simulations, Equation 4 is modified to:

$$540 \quad \text{Scenario value}_{i,t} \\ 541 \quad = \text{TIME}_{i,t} \times \left( \frac{\text{Maximum trajectory value}_i}{\text{Total number of timestep in model}} \right) \\ 542 \quad + (\sigma_i \times \sqrt{dt} \times N(0,1)_t \times \text{Change in Scenario value from default}_{i,t})$$

543  
544 (Equation 5)

545 For Experiment #3 (single slow driver plus noise), the runs were generated in STELLA<sup>39</sup> with the  
 546 following logic: Primary driver active AND Secondary driver remains at default value AND Tertiary  
 547 driver remains at default value AND Noise active. For experiment 4 (noise plus multiple slow  
 548 drivers), the logic used included:

- 549 - Primary driver active AND Secondary driver active AND Tertiary driver remains at default  
550 value AND Noise active
- 551 - Primary driver active AND Secondary driver remains at default value AND Tertiary driver  
552 active AND Noise active
- 553 - Primary driver active AND Secondary driver active AND Tertiary driver active AND Noise  
554 active

555

### 556 3. Timeseries breakpoint detection

557 The identification of the timing of the ATDCs in the model runs was a two-step process.

558

559 First, to ensure that we were only analysing model runs that had transitioned (i.e. collapsed) to  
 560 quantitatively and qualitatively functionally different states (e.g. fishery collapse, civilisation collapse,

561 forest dieback or lake eutrophication), we assessed whether model outcomes had crossed a pre-  
562 defined threshold at any point over the model horizon. For the three models which observe collapses  
563 in the outcome variable (i.e. Lake Chilika fishery, Easter Island and TRIFFID), model runs were  
564 considered to have reached a collapsed state if the outcome variable reached a value beneath 20% of  
565 its initial value at any point during the simulation. This demarcation is therefore representative of  
566 Type-1 boundaries defined by Dearing *et al.*<sup>40</sup>, with the numerical value of the boundary in line with  
567 the concept that fish stocks may be considered collapsed once their biomass falls beneath 20% of the  
568 biomass needed to maintain maximum sustainable yield<sup>65,66</sup>. In the case of the Lake Chilika fishery  
569 model, which has inbuilt social-ecological feedbacks that may trigger the recovery and later re-  
570 collapse of the fishery<sup>21,33</sup>, we subset the timeseries to the period prior to the first timestep beneath  
571 20% of the initial fish population. As we are only interested in the initial collapse, not sub-setting this  
572 time period would risk capturing subsequent collapses and recoveries in the analysis.

573  
574 With lake eutrophication caused by an increase in phosphorus concentrations, a linear threshold  
575 beyond which we could be confident that the model had entered a qualitatively different state could  
576 not be identified. Therefore, as per the approach taken by Drijfhout *et al.*<sup>67</sup> for identifying abrupt  
577 events in global climate models, we adopted a Dearing *et al.*<sup>40</sup> Type-2 boundary to include only  
578 simulations which reached lake phosphorus concentrations greater than four times the standard  
579 deviation (SD) of the pre-ATDC time series. Therefore, runs of the Lake phosphorus model which did  
580 not exceed this 4xSD threshold were not considered to reach phosphorus concentrations sufficiently  
581 outside of the pre-transition envelope of variability, and were therefore excluded from our analysis.

582  
583 The second stage of timeseries breakpoint detection used the optimal breakpoint function of the R  
584 package 'strucchange' v.1.5-2<sup>68</sup> to identify ATDC dates in the time series that had successfully met the  
585 above qualifications (i.e. reached an alternative state). As described in Cooper *et al.*<sup>21</sup>, the optimal  
586 breakpoint function finds the most significant deviation from stability in classical regression models  
587 (Figure S3-2), whereby regressions coefficients shift from one regime to another. Therefore, the  
588 breakpoint date is taken as the most significant deviation of the outcome variable *en route* to its  
589 qualitatively and quantitatively alternative state.

590

#### 591 4. Boxplots and output graphs

592 For each of the experiments (i.e. Methods Sections 2.1-2.3), boxplots were generated to visualise the  
593 distribution of breakpoint dates for each of the slow driver and noise level combinations (Figures 2-  
594 4). To standardise the comparisons between experiments, the normalised magnitude (0 → 1) of the  
595 primary trajectories (Table S3-2) for each model was plotted on the horizontal axes. In turn, to  
596 visualise how the breakpoint dates change with the addition of secondary or noisy stresses over the  
597 range of the primary trajectories, model outcomes that tipped (Methods Sections 3.1-3.2) were subset  
598 in the statistical software R between normalised primary trajectory values of 0.25-0.35, 0.45-0.55, and  
599 0.65-0.75. From here, boxplots for each of the driver combinations (e.g. 'primary only', 'primary and  
600 secondary', etc.) and primary driver subsets (e.g. 0.25-0.35, 0.45-0.55 etc.) were graphed in R using  
601 the package 'ggplot' [v.3.3.5<sup>69</sup>].

602

#### 603 **Data Availability Statement**

604 The datasets generated during and/or analysed during the current study are available from the  
605 corresponding author on reasonable request, with the models used to create these data available in  
606 a DOI-minting repository: <https://doi.org/10.5281/zenodo.7946433>.

607

#### 608 **Code Availability Statement**

609 The code used to analyse the modelled data are deposited in a DOI-minting repository:  
610 <https://doi.org/10.5281/zenodo.7946433>.

611

#### 612 **Acknowledgments**

613 SW received funding from NE/W005050/1, NE/T00391X/1, ES/T007877/1, ES/R009279/1,  
614 AH/W003813/1, and BB/X010961/1. GSC received funding by the UKRI-GCRF Action Against Stunting  
615 Hub (Project ref. MR/S01313X/1).

616

#### 617 **Author Contributions Statement**

618 SW, GSC and JAD conceived and wrote the manuscript. GSC ran and analysed the models. JA provided  
619 statistically support and conceptualised the figures. All authors edited and approved the final  
620 manuscript.

621

#### 622 **Competing Interests Statement**

623 The authors declare no competing interests.

624

#### 625 **Inclusion and Ethics Statement**

626 This research is global in scope, using models that have been appropriately cited throughout. Roles  
627 and responsibilities were agreed amongst collaborators ahead of the research.

628

#### 629 **Figure Legends/Captions (for main text figures)**

630

631 **Figure 1: Schematic overview of the framework developed to explore the influence of slow driver**  
632 **trajectories and/or noise on the timing of abrupt threshold-dependent changes (ATDCs):** (A) *the four*  
633 *systems models simulated in this study (Methods Section 1); (B) schematic representation of a system*  
634 *dynamics model (Lake phosphorus model) with its external slow (blue and green) and noisy (red/orange)*  
635 *drivers depicted in colour (Methods Section 2); (C) depiction of the four experiment types (Methods*  
636 *Sections 2.1-2.3), ranging from changes in the primary baseline driver only (Experiment #1), changes in*  
637 *all slow drivers and noise inputs simultaneously (Experiment #4, where ‘a’ and ‘b’ represent noise profiles*  
638 *that are uncoupled or coupled to the primary driver trajectory, respectively): darker colours*  
639 *schematically represent steeper trajectories and/or higher noise levels; (D) the two linear techniques*  
640 *used to check whether outcomes shift into a functionally different state (Methods Section 3.1) – the top*  
641 *panel is applied to Lake Chilika, Easter Island and TRIFFID, where the systems collapse from high*  
642 *quantitative outcome states to low quantitative outcome states, and the bottom panel is applied to Lake*  
643 *phosphorus (where lake phosphorus concentrations shift from low to high); (E) depiction of the*  
644 *timeseries breakpoint date recognition (Methods Section 3.1). The Easter Island icon in (A) is made by*  
645 *Roundicons and the remaining three icons are made by Freekpiik, as sourced from www.flaticon.com*  
646

647

648 **Figure 2 – The relationship between the breakpoint date and the primary (baseline) slow driver for the**  
649 **individual (grey) and multiple (coloured) drivers.** *The normalised primary driver trajectories are*  
650 *apportioned into three discrete ranges: ‘low’ – 0.25-0.35, ‘mid’ – 0.45-0.55, and ‘high’ – 0.65-0.75. .*  
651 *Subplots: (A) Lake Chilika model, primary slow driver: fisher population growth, secondary driver:*  
652 *climate change, tertiary driver: fish price; (B) Easter Island model, primary slow driver = tree clearance,*  
653 *secondary driver: agricultural carrying capacity, tertiary driver: tree mortality; (C) TRIFFID model,*  
654 *primary slow driver: temperature change, secondary driver: disturbance rate; (D) Lake phosphorus*  
655 *model, primary slow driver: phosphorus external input, secondary driver: phosphorus recycling rate,*  
656 *tertiary driver: phosphorus sedimentation rate. Model timestep units: Lake Chilika, Easter Island and*  
657 *TRIFFID run in years; timesteps in Lake phosphorus are unitless. Boxplots depict the median (50<sup>th</sup>*  
658 *percentile), upper quartile (75<sup>th</sup> percentile) and lower quartile (25<sup>th</sup> percentile); individual points*  
659 *represent outliers which fall outside 1.5 times the interquartile range from the lower and upper quartiles*  
660 *(as depicted by the boxplot whiskers). See Table S3-1 for the number of model simulations underpinning*  
661 *each boxplot.*

662

663 **Figure 3 – The relationship between the breakpoint date and the primary slow driver (grey) for varying**  
664 **levels of uncoupled noise in the primary slow driver ( $\sigma$ ), where normalised  $\sigma$  values  $\leq 0.333$  signify ‘low**

664 noise' (yellow), normalised  $\sigma$  values  $> 0.333$  and  $\leq 0.666$  signify 'mid noise' (orange), and normalised  $\sigma$   
665 values  $> 0.666$  signify 'high noise' (red; Methods Section 2.3). The normalised primary driver trajectories  
666 are apportioned into three discrete ranges: 'low' – 0.25-0.35, 'mid' – 0.45-0.55, and 'high' – 0.65-0.75.  
667 Subplots: (A) Chilika model outputs, primary slow driver = fisher population growth; (B) Easter Island  
668 model outputs, primary slow driver = tree clearance; (C) TRIFFID model outputs, primary slow driver =  
669 temperature change; (D) Lake phosphorus model outputs, primary slow driver = phosphorus input.  
670 Model timestep units and boxplot dimensions are the same as in Figure 2; see Table S3-1 for the number  
671 of model simulations underpinning each boxplot.

672

673 **Figure 4 – The relationship between the breakpoint date and the primary slow driver (grey) when weak**  
674 **(normalised T values  $\leq 0.333$ ) and strong (normalised T values  $> 0.666$ ) multiple driver trajectories are**  
675 **combined with weak (normalised  $\sigma$  values  $\leq 0.333$ ) and strong (normalised  $\sigma$  values  $> 0.666$ ) uncoupled**  
676 **noise (T = trajectory, N = noise). The normalised primary driver trajectories are apportioned into three**  
677 **discrete ranges: 'low' – 0.25-0.35, 'mid' – 0.45-0.55, and 'high' – 0.65-0.75. . Subplots: (A) the Chilika**  
678 **model, primary slow driver = fisher population growth, additional driver: climate change and fish price;**  
679 **(B) the Easter Island model, primary slow driver = tree clearance, additional drivers: agricultural carrying**  
680 **capacity and tree mortality; (C) the TRIFFID model, primary slow driver = temperature change, additional**  
681 **driver: disturbance rate; (D) the Lake phosphorus model, primary slow driver = phosphorus, additional**  
682 **drivers: phosphorus recycling rate, phosphorus sedimentation rate. Note, the Lake phosphorus model**  
683 **(subplot D) did not produce any outcomes between the 0.65-0.75 primary driver range within the 'high**  
684 **trajectory, high noise' scenario; however, the median breakpoint date of the adjacent range (0.55-0.65)**  
685 **is 346. Model timestep units and boxplot dimensions are the same as in Figure 2; see Table S3-1 for the**  
686 **number of model simulations underpinning each boxplot.**

687

## 688 **References**

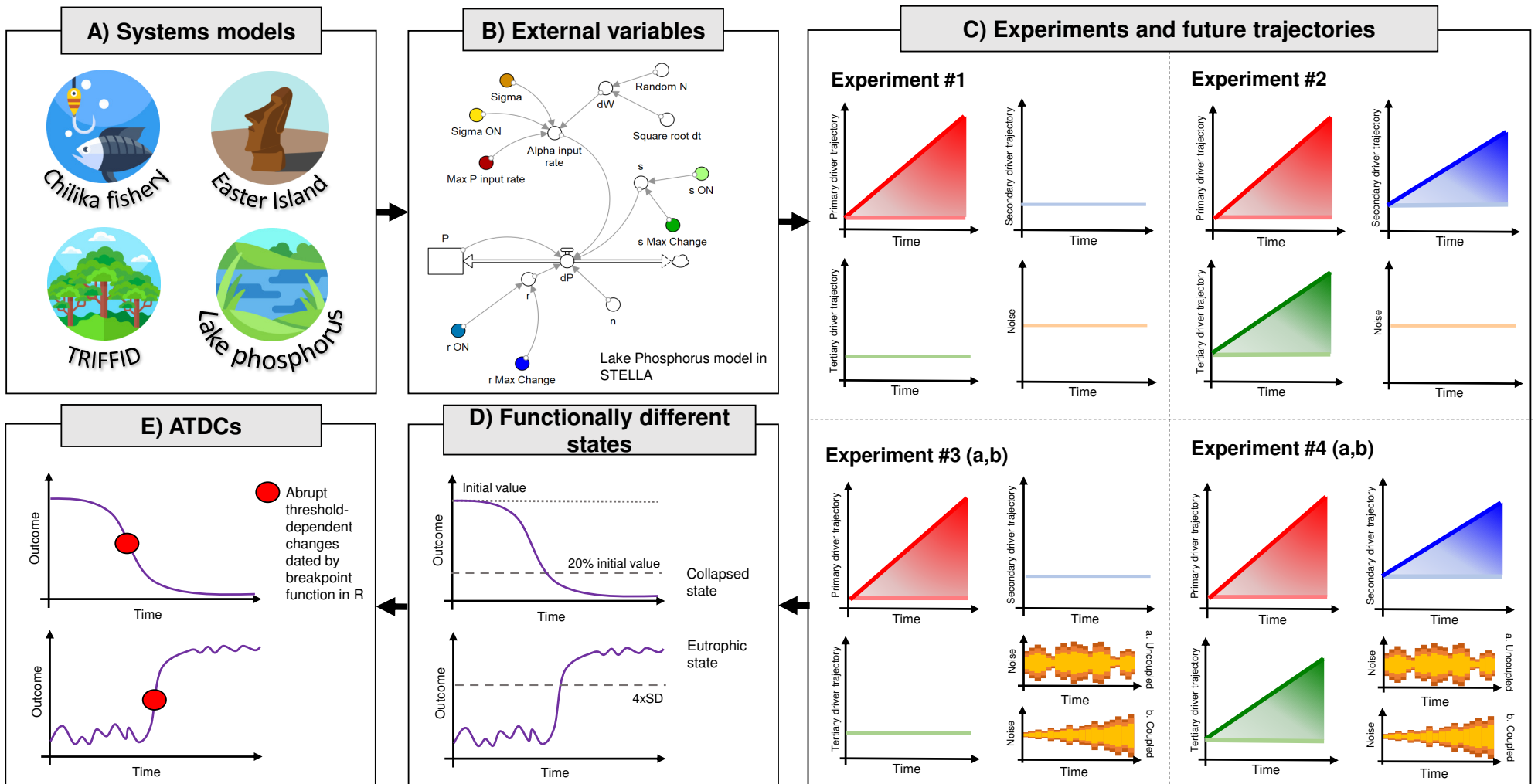
- 689 1. Beddington, J. *Food, Energy, Water and the Climate: A Perfect Storm of global events.* (2009).
- 690 2. Bradshaw, C. J. A. *et al.* Underestimating the Challenges of Avoiding a Ghastly Future. *Front.*  
691 *Conserv. Sci.* **0**, 9 (2021).
- 692 3. Retsa, A., Schelske, O., Wilke, B., Rutherford, G. & de Jong, R. *Biodiversity and Ecosystem*  
693 *Services A business case for re/insurance.*  
694 [https://www.swissre.com/institute/research/topics-and-risk-dialogues/climate-and-natural-](https://www.swissre.com/institute/research/topics-and-risk-dialogues/climate-and-natural-catastrophe-risk/expertise-publication-biodiversity-and-ecosystems-services)  
695 [catastrophe-risk/expertise-publication-biodiversity-and-ecosystems-services](https://www.swissre.com/institute/research/topics-and-risk-dialogues/climate-and-natural-catastrophe-risk/expertise-publication-biodiversity-and-ecosystems-services) (2020).
- 696 4. Reichstein, M., Riede, F. & Frank, D. More floods, fires and cyclones — plan for domino  
697 effects on sustainability goals. *Nat.* **2021 5927854 592**, 347–349 (2021).
- 698 5. Scheffer, M. *et al.* Anticipating Critical Transitions. *Science (80- ).* **338**, 344–348 (2012).
- 699 6. Kareiva, P. & Carranza, V. Existential risk due to ecosystem collapse: Nature strikes back.  
700 *Futures* **102**, 39–50 (2018).
- 701 7. Kemp, L. *et al.* Climate Endgame: Exploring catastrophic climate change scenarios. *Proc. Natl.*  
702 *Acad. Sci.* **119**, e2108146119 (2022).
- 703 8. Steffen, W. *et al.* Planetary boundaries: Guiding human development on a changing planet.  
704 *Science (80- ).* **347**, (2015).
- 705 9. Ripple, W. J., Wolf, C., Newsome, T. M., Barnard, P. & Moomaw, W. R. World Scientists'  
706 Warning of a Climate Emergency. *Bioscience* **70**, 8–12 (2020).
- 707 10. Secretariat of the Convention on Biological Diversity. *Global Biodiversity Outlook 5.*  
708 [www.cbd.int/GBO5](http://www.cbd.int/GBO5) (2020).
- 709 11. IPCC. Summary for Policymakers. in *Climate Change 2021: The Physical Science Basis.*  
710 *Contribution of Working Group I to the Sixth Assessment Report of the Intergovernmental*  
711 *Panel on Climate Change* (eds. Masson-Delmotte *et al.*) 1–3949 (Cambridge University Press,  
712 2021).
- 713 12. Büntgen, U. *et al.* Recent European drought extremes beyond Common Era–background  
714 variability. *Nat. Geosci.* **2021 144 14**, 190–196 (2021).

- 715 13. Abram, N. J. *et al.* Connections of climate change and variability to large and extreme forest  
716 fires in southeast Australia. *Commun. Earth Environ.* 2021 21 2, 1–17 (2021).
- 717 14. Toreti, A., Cronie, O. & Zampieri, M. Concurrent climate extremes in the key wheat producing  
718 regions of the world. *Sci. Reports* 2019 91 9, 1–8 (2019).
- 719 15. Vogel, M. M., Hauser, M. & Seneviratne, S. I. Projected changes in hot, dry and wet extreme  
720 events' clusters in CMIP6 multi-model ensemble. *Environ. Res. Lett.* 15, 094021 (2020).
- 721 16. Gaupp, F., Hall, J., Mitchell, D. & Dadson, S. Increasing risks of multiple breadbasket failure  
722 under 1.5 and 2 °C global warming. *Agric. Syst.* 175, 34–45 (2019).
- 723 17. McKay, D. I. A. *et al.* Exceeding 1.5°C global warming could trigger multiple climate tipping  
724 points. *Science (80-. )*. 377, (2022).
- 725 18. Siteur, K., Eppinga, M. B., Doelman, A., Siero, E. & Rietkerk, M. Ecosystems off track: rate-  
726 induced critical transitions in ecological models. *Oikos* 125, 1689–1699 (2016).
- 727 19. Ashwin, P., Wieczorek, S., Vitolo, R. & Cox, P. Tipping points in open systems: bifurcation,  
728 noise-induced and rate-dependent examples in the climate system. *Philos. Trans. R. Soc. A*  
729 *Math. Phys. Eng. Sci.* 370, 1166–1184 (2012).
- 730 20. O'Keeffe, P. E. & Wieczorek, S. Tipping Phenomena and Points of No Return in Ecosystems:  
731 Beyond Classical Bifurcations. *SIAM J. Appl. Dyn. Syst.* 19, 2371–2402 (2019).
- 732 21. Cooper, G. S., Willcock, S. & Dearing, J. A. Regime shifts occur disproportionately faster in  
733 larger ecosystems. *Nat. Commun.* 11, (2020).
- 734 22. Arani, B. M. S., Carpenter, S. R., Lahti, L., Van Nes, E. H. & Scheffer, M. Exit time as a measure  
735 of ecological resilience. *Science (80-. )*. 372, (2021).
- 736 23. Thompson, J. M. T. & Sieber, J. Predicting Climate Tipping as a noisy bifurcation: A Review.  
737 *Int. J. Bifurc. Chaos* 21, 399–423 (2011).
- 738 24. Wilson, W. G. Resolving discrepancies between deterministic population models and  
739 individual-based simulations. *Am. Nat.* 151, 116–134 (1998).
- 740 25. Thompson, R. M., Beardall, J., Beringer, J., Grace, M. & Sardina, P. Means and extremes:  
741 building variability into community-level climate change experiments. *Ecol. Lett.* 16, 799–806  
742 (2013).
- 743 26. Kreyling, J., Jentsch, A. & Beier, C. Beyond realism in climate change experiments: gradient  
744 approaches identify thresholds and tipping points. *Ecol. Lett.* 17, 125-e1 (2014).
- 745 27. Ritchie, P. D. L., Clarke, J. J., Cox, P. M. & Huntingford, C. Overshooting tipping point  
746 thresholds in a changing climate. *Nat.* 2021 5927855 592, 517–523 (2021).
- 747 28. Wang, R. *et al.* Flickering gives early warning signals of a critical transition to a eutrophic lake  
748 state. *Nature* 492, 419–422 (2012).
- 749 29. Groffman, P. M. *et al.* Ecological thresholds: The key to successful environmental  
750 management or an important concept with no practical application? *Ecosystems* 9, 1–13  
751 (2006).
- 752 30. Renaud, F. G., Birkmann, J., Damm, M. & Gallopín, G. C. Understanding multiple thresholds of  
753 coupled social–ecological systems exposed to natural hazards as external shocks. *Nat.*  
754 *Hazards* 55, 749–763 (2010).
- 755 31. Kelly, R. A. *et al.* Selecting among five common modelling approaches for integrated  
756 environmental assessment and management. *Environ. Model. Softw.* 47, 159–181 (2013).
- 757 32. Filatova, T., Polhill, J. G. & van Ewijk, S. Regime shifts in coupled socio-environmental  
758 systems: Review of modelling challenges and approaches. *Environ. Model. Softw.* 75, 333–  
759 347 (2016).
- 760 33. Cooper, G. S. & Dearing, J. A. Modelling future safe and just operating spaces in regional  
761 social-ecological systems. *Sci. Total Environ.* 651, 2105–2117 (2019).
- 762 34. Tenza, A., Pérez, I., Martínez-Fernández, J. & Giménez, A. Understanding the decline and  
763 resilience loss of a long-lived social-ecological system: insights from system dynamics. *Ecol.*  
764 *Soc. Publ. online May 02, 2017 | doi10.5751/ES-09176-220215* 22, (2017).
- 765 35. Martin, R. & Schlüter, M. Combining system dynamics and agent-based modeling to analyze

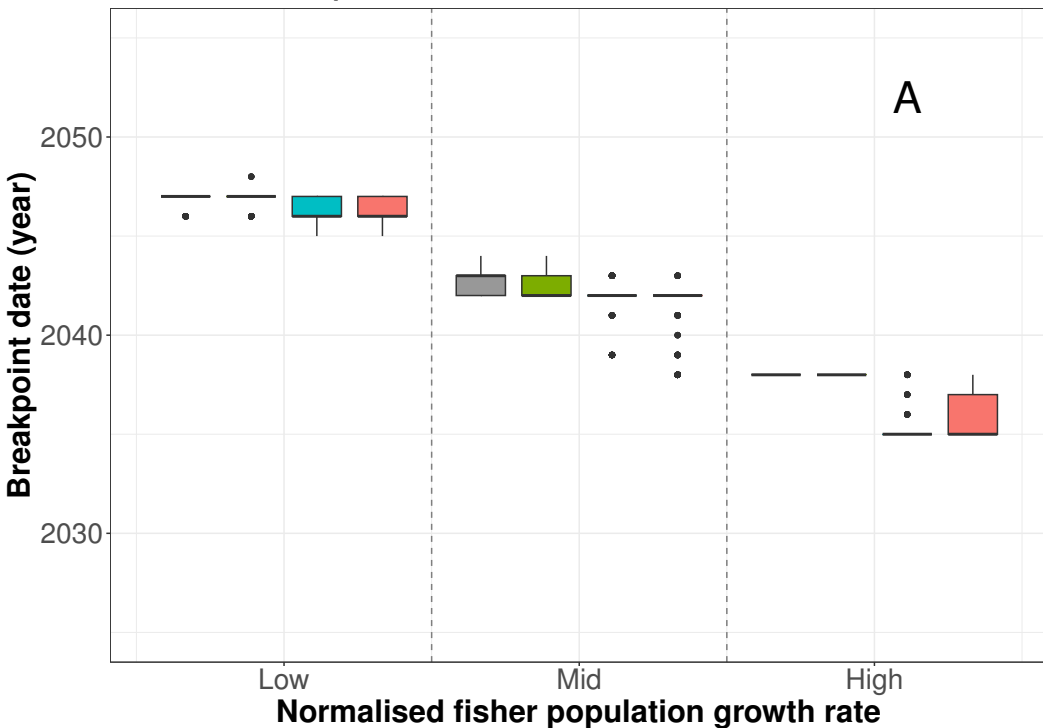


- 766 social-ecological interactions-an example from modeling restoration of a shallow lake. *Front.*  
767 *Environ. Sci.* **3**, 66 (2015).
- 768 36. Brandt, G. & Merico, A. The slow demise of Easter Island: Insights from a modeling  
769 investigation. *Front. Ecol. Evol.* **3**, 13 (2015).
- 770 37. Carpenter, S. R., Ludwig, D. & Brock, W. A. Management of eutrophication for lakes subject to  
771 potentially irreversible change. *Ecol. Appl.* **9**, 751–771 (1999).
- 772 38. Cox, P. M. *et al.* Amazonian forest dieback under climate-carbon cycle projections for the  
773 21st century. *Theor. Appl. Climatol.* **2004 781 78**, 137–156 (2004).
- 774 39. ISEE Systems. STELLA Architect: Systems Thinking for Education and Research. at  
775 <https://www.iseesystems.com/about.aspx%0A> (2018).
- 776 40. Dearing, J. A. *et al.* Safe and just operating spaces for regional social-ecological systems. *Glob.*  
777 *Environ. Chang.* **28**, 227–238 (2014).
- 778 41. Krönke, J. *et al.* Dynamics of tipping cascades on complex networks. *Phys. Rev. E* **101**, 042311  
779 (2020).
- 780 42. Kinzig, A. P. *et al.* Resilience and regime shifts: assessing cascading effects. *Ecol. Soc.* **11**, 1–23  
781 (2006).
- 782 43. Klose, A. K., Karle, V., Winkelmann, R. & Donges, J. F. Emergence of cascading dynamics in  
783 interacting tipping elements of ecology and climate. *R. Soc. Open Sci.* **7**, 200599 (2020).
- 784 44. Wang, R., Dearing, J. A. & Langdon, P. G. Critical transitions in ecosystem state are driven by  
785 coupled feedback mechanisms: a case study from Erhai lake, China. *Water* **13**, (2021).
- 786 45. Rietkerk, M. *et al.* Evasion of tipping in complex systems through spatial pattern formation.  
787 *Science (80-. )*. **374**, (2021).
- 788 46. Bastiaansen, R., Dijkstra, H. A. & Von Der Heydt, A. S. Fragmented tipping in a spatially  
789 heterogeneous world. *Environ. Res. Lett.* **17**, 045006 (2022).
- 790 47. Dearing, J. A. *et al.* Navigating the perfect storm: Research strategies for social ecological  
791 systems in a rapidly evolving world. *Environ. Manage.* **49**, 767–775 (2011).
- 792 48. Verburg, P. H. *et al.* Methods and approaches to modelling the Anthropocene. *Glob. Environ.*  
793 *Chang.* **39**, 328–340 (2016).
- 794 49. Beven, K. A manifesto for the equifinality thesis. *J. Hydrol.* **320**, 18–36 (2006).
- 795 50. Reisinger, D. & Füllsack, M. Comparing Equation-Based and Agent-Based Data Generation  
796 Methods for Early Warning Signal Analysis. *Syst. 2020, Vol. 8, Page 54* **8**, 54 (2020).
- 797 51. Scheffer, M. *et al.* Early-warning signals for critical transitions. *Nature* **461**, 53–9 (2009).
- 798 52. Bury, T. M. *et al.* Deep learning for early warning signals of tipping points. *Proc. Natl. Acad.*  
799 *Sci. U. S. A.* **118**, (2021).
- 800 53. Doncaster, C. P. *et al.* Early warning of critical transitions in biodiversity from compositional  
801 disorder. *Ecology* **97**, 3079–3090 (2016).
- 802 54. Wang, R. *et al.* Network parameters quantify loss of assemblage structure in human-  
803 impacted lake ecosystems. *Glob. Chang. Biol.* **25**, 3871–3882 (2019).
- 804 55. Mayfield, R. J. *et al.* Metrics of structural change as indicators of chironomid community  
805 stability in high latitude lakes. *Quat. Sci. Rev.* **249**, 106594 (2020).
- 806 56. Cai, Y., Lenton, T. M. & Lontzek, T. S. Risk of multiple interacting tipping points should  
807 encourage rapid CO2 emission reduction. *Nat. Clim. Chang.* **2016 65 6**, 520–525 (2016).
- 808 57. Dietz, S., Rising, J., Stoerk, T. & Wagner, G. Economic impacts of tipping points in the climate  
809 system. *Proc. Natl. Acad. Sci. U. S. A.* **118**, (2021).
- 810 58. Fabbri, S., Hauschild, M. Z., Lenton, T. M. & Owsianiak, M. Multiple climate tipping points  
811 metrics for improved sustainability assessment of products and services. *Environ. Sci.*  
812 *Technol.* **55**, 2800–2810 (2021).
- 813 59. Steffen, W., Broadgate, W., Deutsch, L., Gaffney, O. & Ludwig, C. The trajectory of the  
814 Anthropocene: The Great Acceleration: *Anthr. Rev.* **2**, 81–98 (2015).
- 815 60. R Core Team. R: A language and environment for statistical computing. at [https://www.r-](https://www.r-project.org/)  
816 [project.org/](https://www.r-project.org/) (2020).

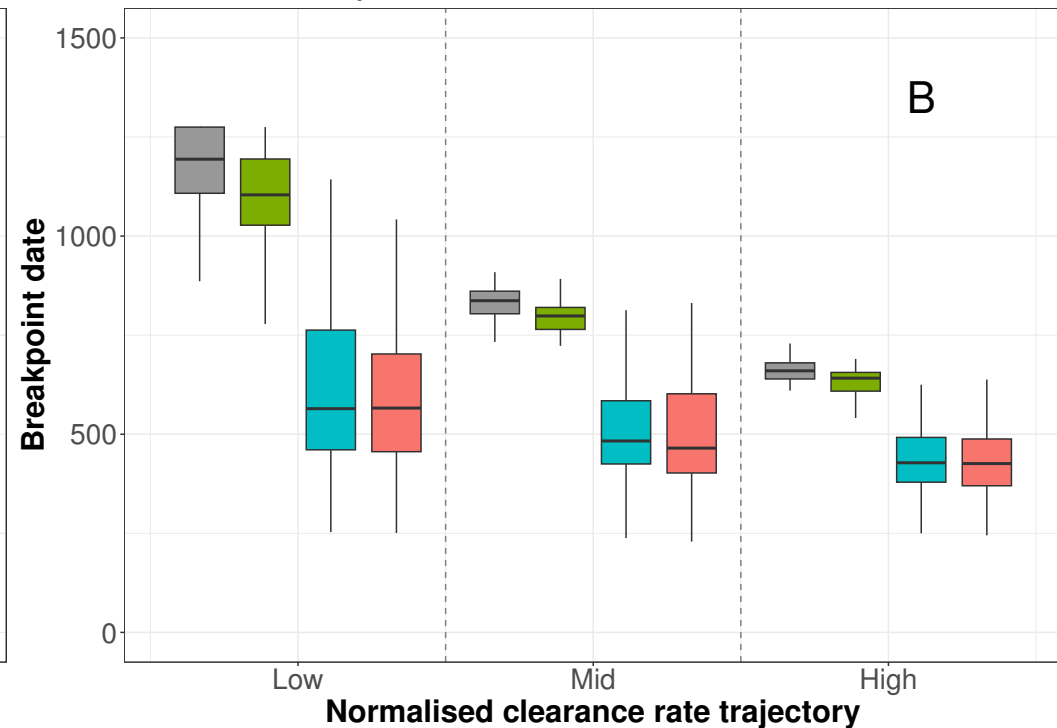
- 817 61. Carpenter, S. R. Eutrophication of aquatic ecosystems: Bistability and soil phosphorus. *Proc.*  
818 *Natl. Acad. Sci. U. S. A.* **102**, 10002–10005 (2005).
- 819 62. Rheinboldt, W. C. Methods for Solving Systems of Nonlinear Equations. *Methods Solving Syst.*  
820 *Nonlinear Equations* (1998) doi:10.1137/1.9781611970012.
- 821 63. Huang, S., Zhang, K., Lin, Q., Liu, J. B. & Shen, J. Abrupt ecological shifts of lakes during the  
822 Anthropocene. *Earth-Science Rev.* **227**, 103981 (2022).
- 823 64. IPCC. Climate Change 2013: The Physical Science Basis. in *Contribution of Working Group I to*  
824 *the Fifth Assessment Report of the Intergovernmental Panel on Climate Change* (eds. Stocker,  
825 T. F. et al.) 1535 (Cambridge University Press, 2013).
- 826 65. Worm, B. *et al.* Rebuilding Global Fisheries. *Science (80-. )*. **325**, 578–585 (2009).
- 827 66. Pinsky, M. L., Jensen, O. P., Ricard, D. & Palumbi, S. R. Unexpected patterns of fisheries  
828 collapse in the world’s oceans. *Proc. Natl. Acad. Sci. U. S. A.* **108**, 8317–8322 (2011).
- 829 67. Drijfhout, S. *et al.* Catalogue of abrupt shifts in Intergovernmental Panel on Climate Change  
830 climate models. *Proc. Natl. Acad. Sci. U. S. A.* **112**, E5777–E5786 (2015).
- 831 68. Zeileis, A., Leisch, F., Hornik, K. & Kleiber, C. Package “strucchange”. [https://cran.r-](https://cran.r-project.org/web/packages/strucchange/strucchange.pdf)  
832 [project.org/web/packages/strucchange/strucchange.pdf](https://cran.r-project.org/web/packages/strucchange/strucchange.pdf) (2015).
- 833 69. Wickham, H. ggplot2: Elegant Graphics for Data Analysis. at [https://doi.org/978-3-319-24277-](https://doi.org/978-3-319-24277-4)  
834 [4](https://doi.org/978-3-319-24277-4) (2016).
- 835



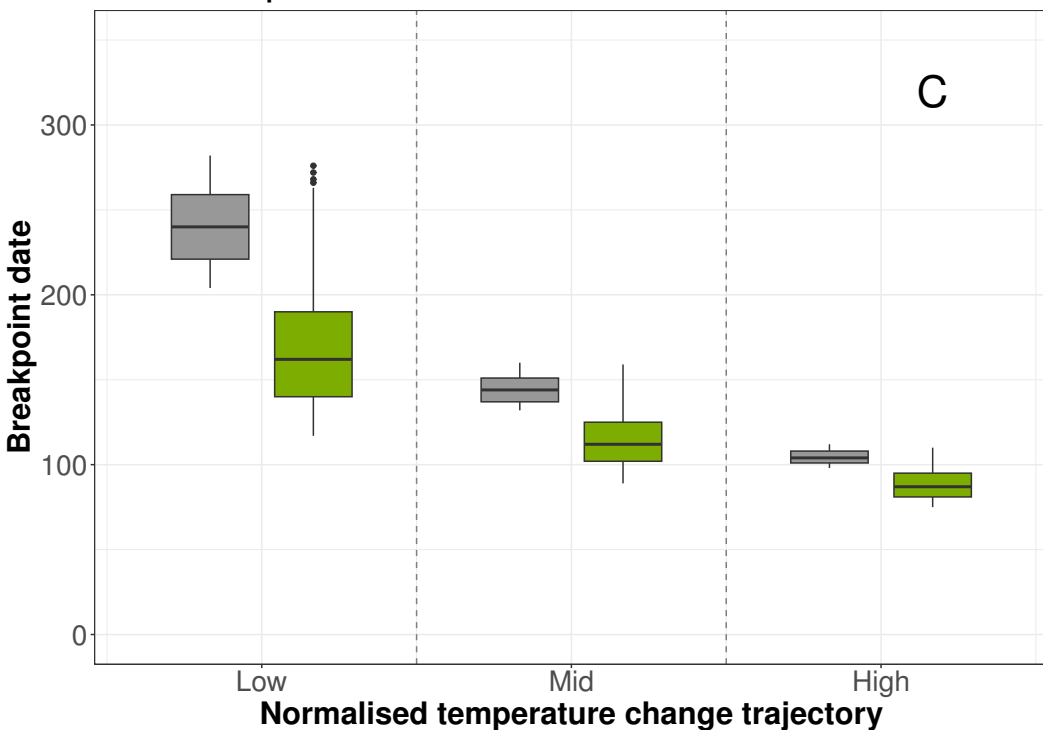
Lake Chilika: Multiple slow rates



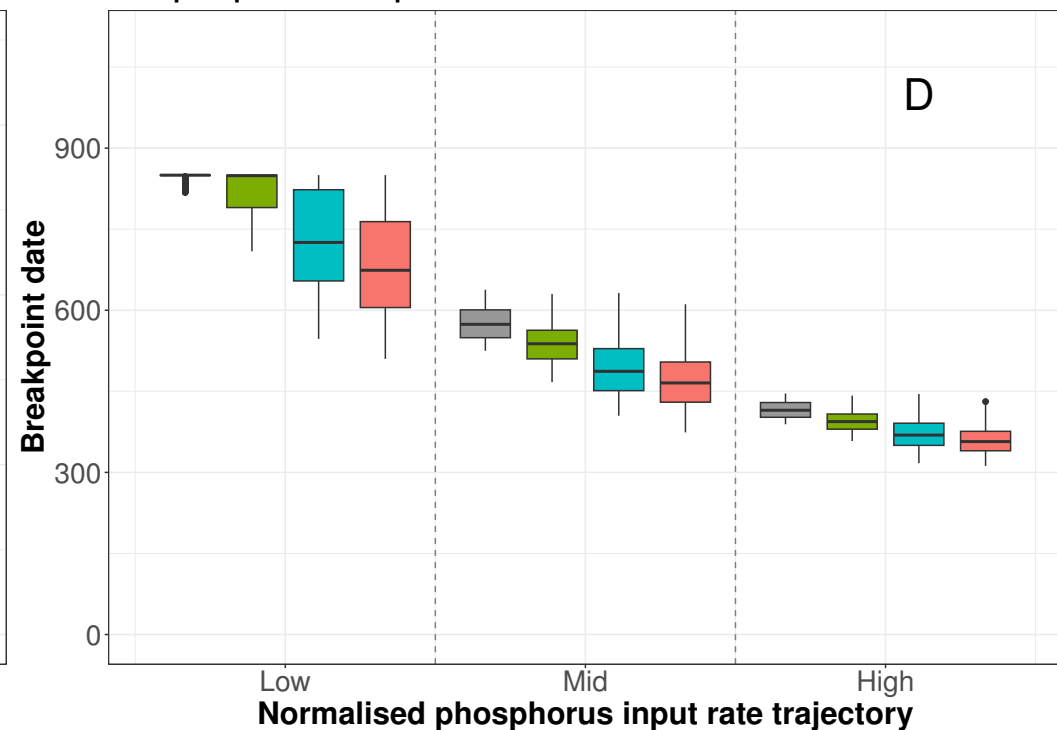
Easter Island: Multiple slow rates



TRIFFID: Multiple slow rates

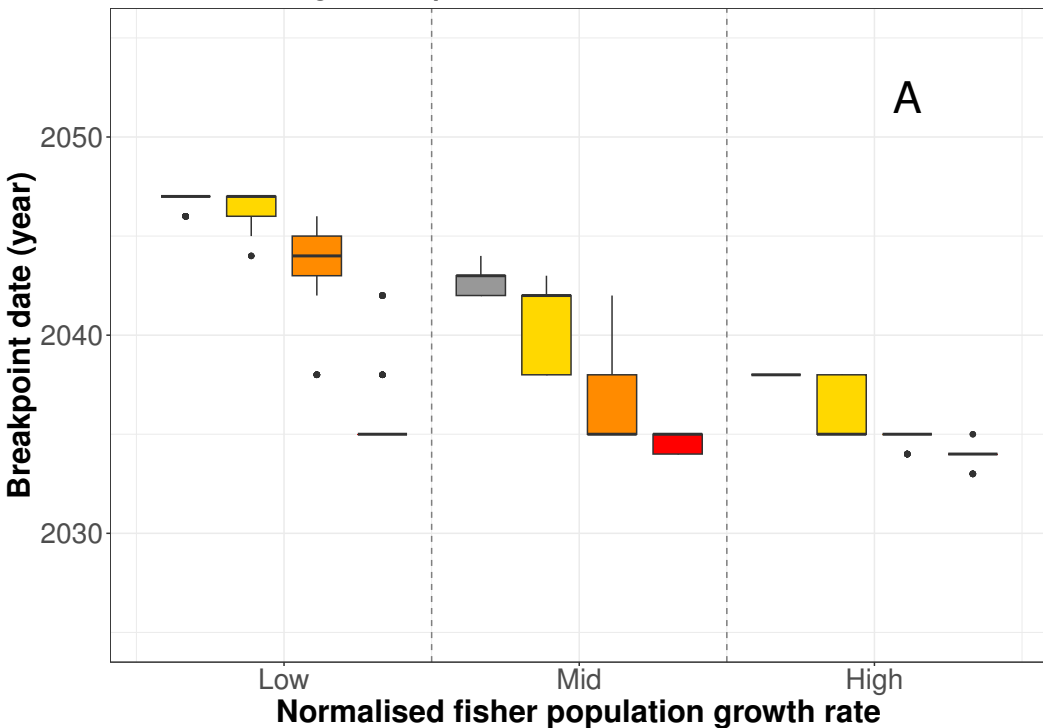


Lake phosphorus: Multiple slow rates

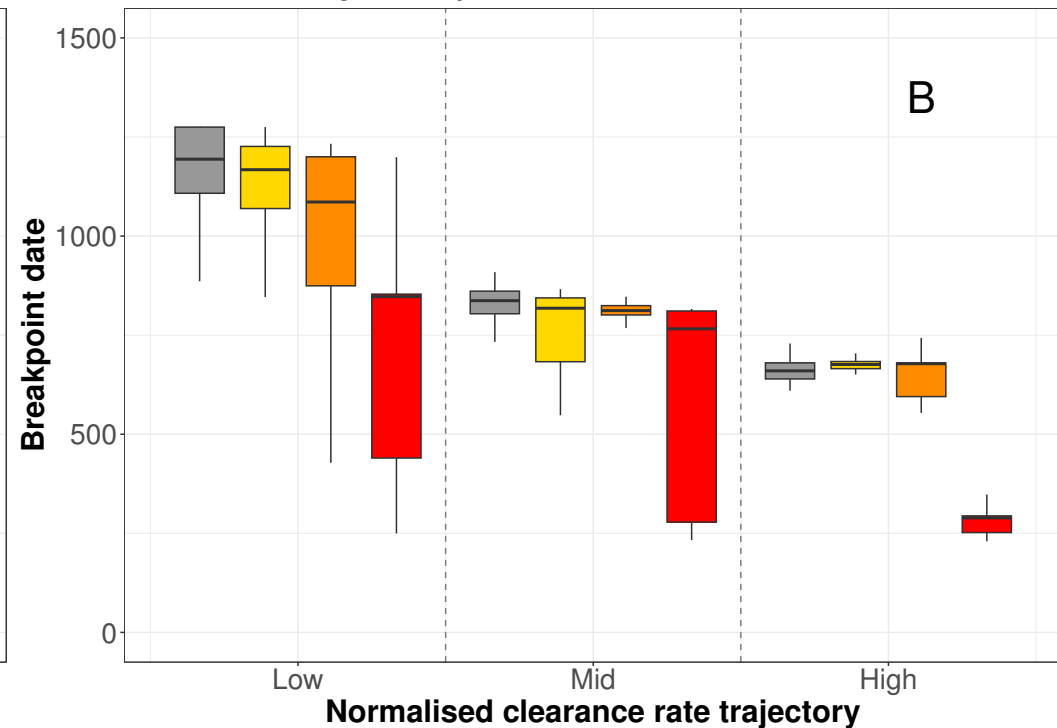


Scenario ■ Baseline ■ Secondary ■ Tertiary ■ All

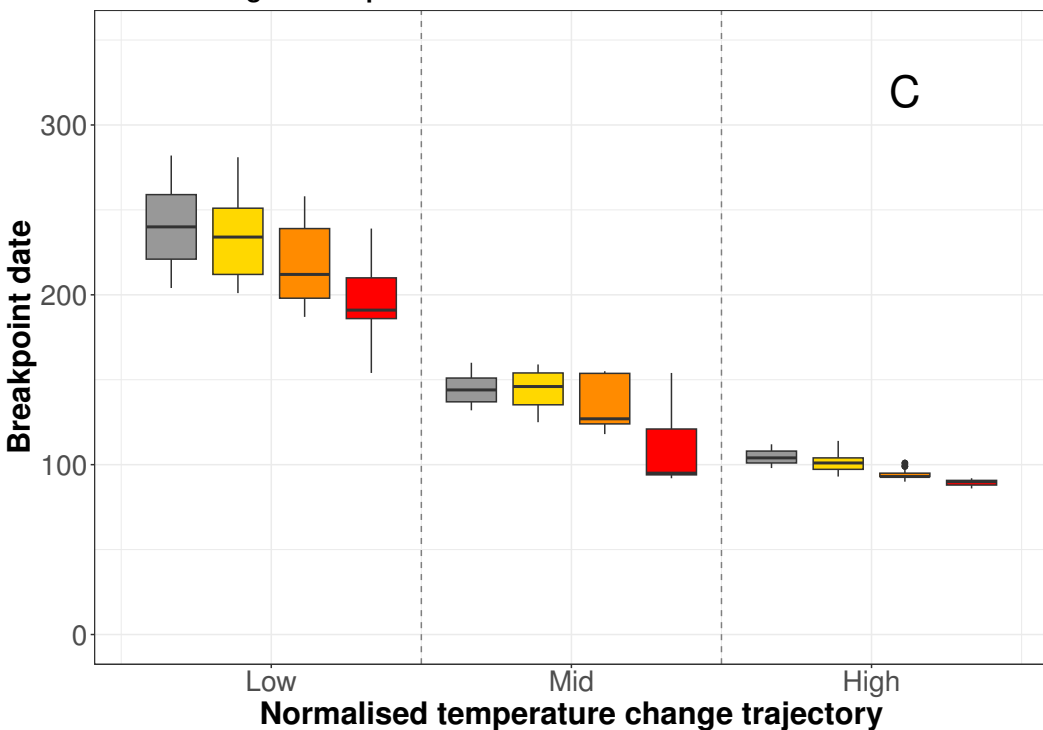
Lake Chilika: Single uncoupled noise



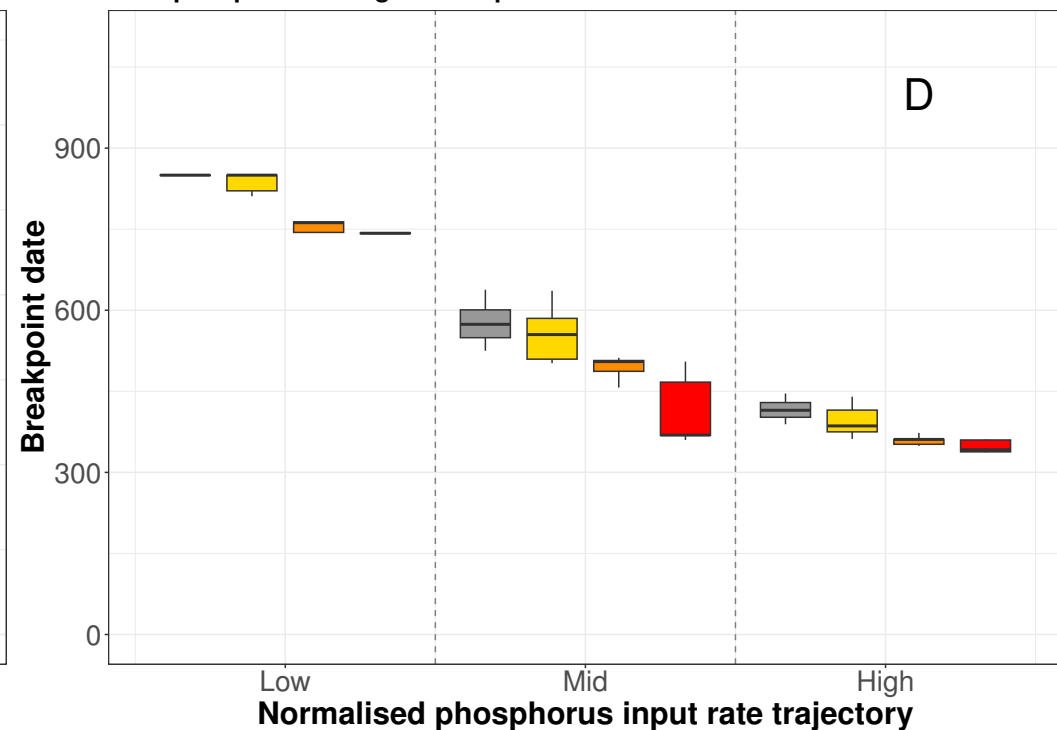
Easter Island: Single uncoupled noise



TRIFFID: Single uncoupled noise

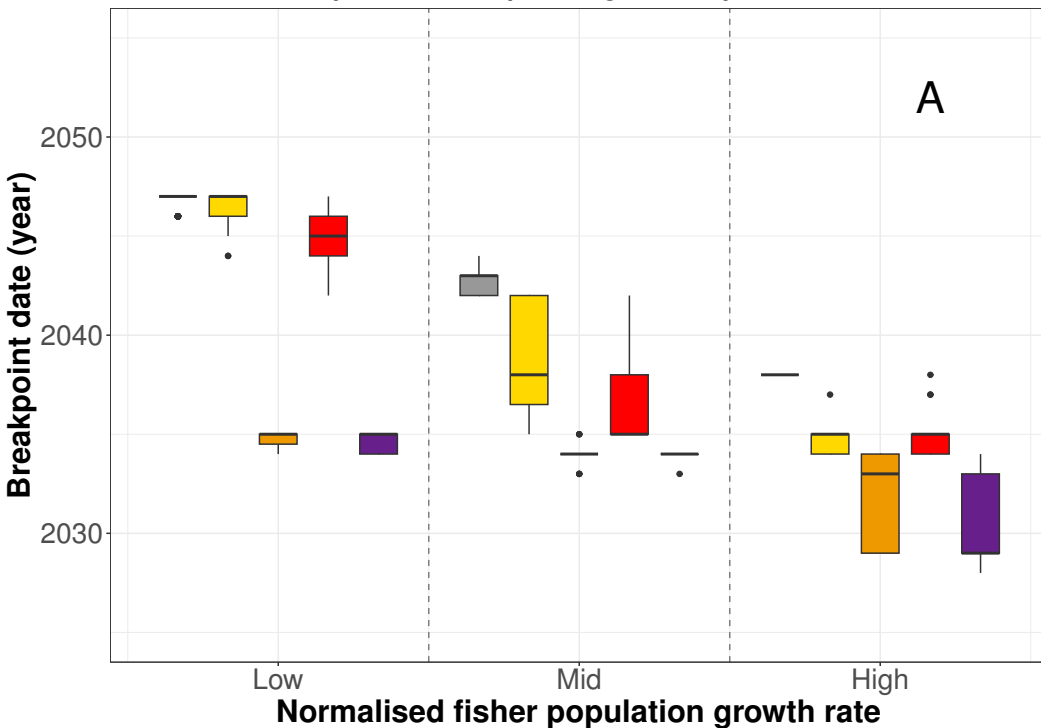


Lake phosphorus: Single uncoupled noise

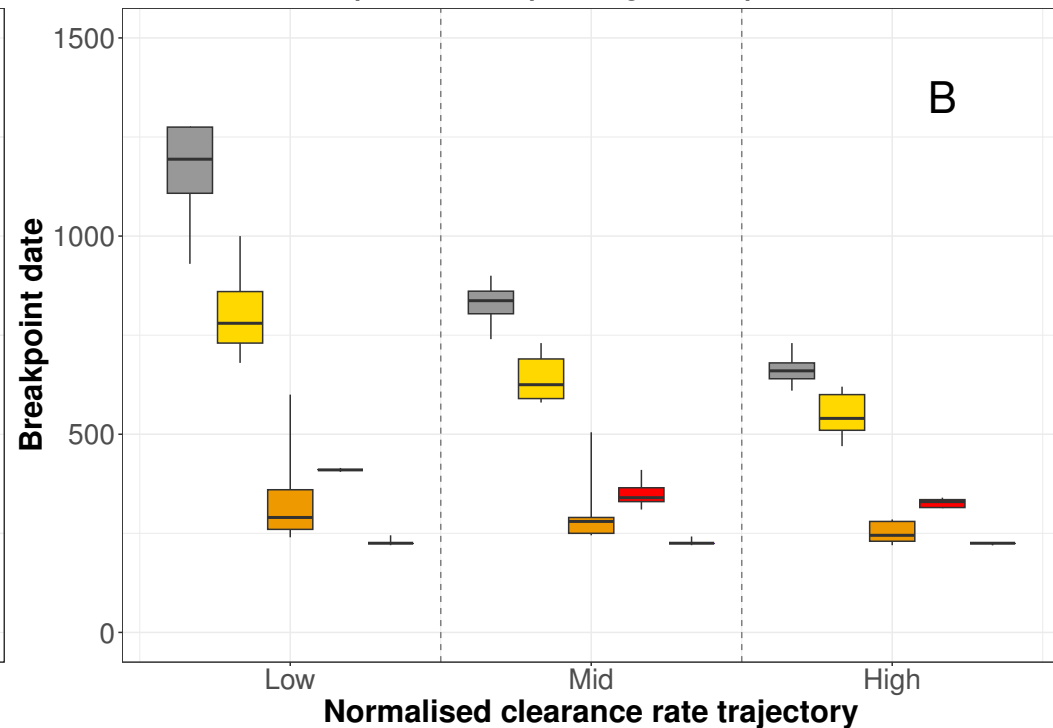


Noise Baseline Low Mid High

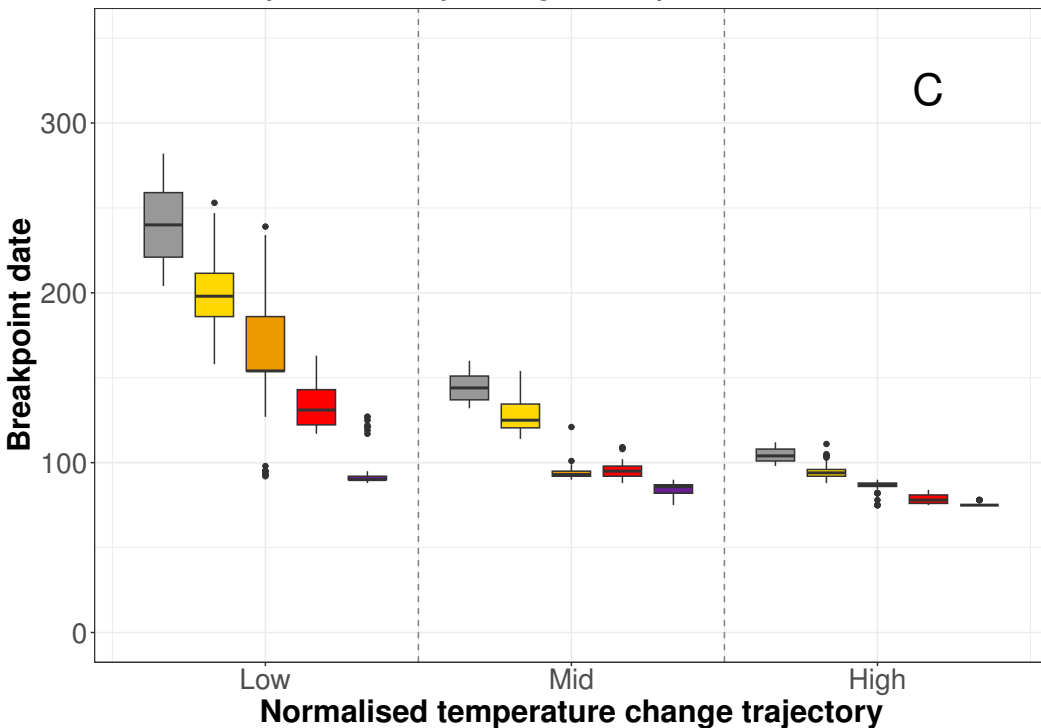
Lake Chilika: Multiple slow rates plus single uncoupled noise



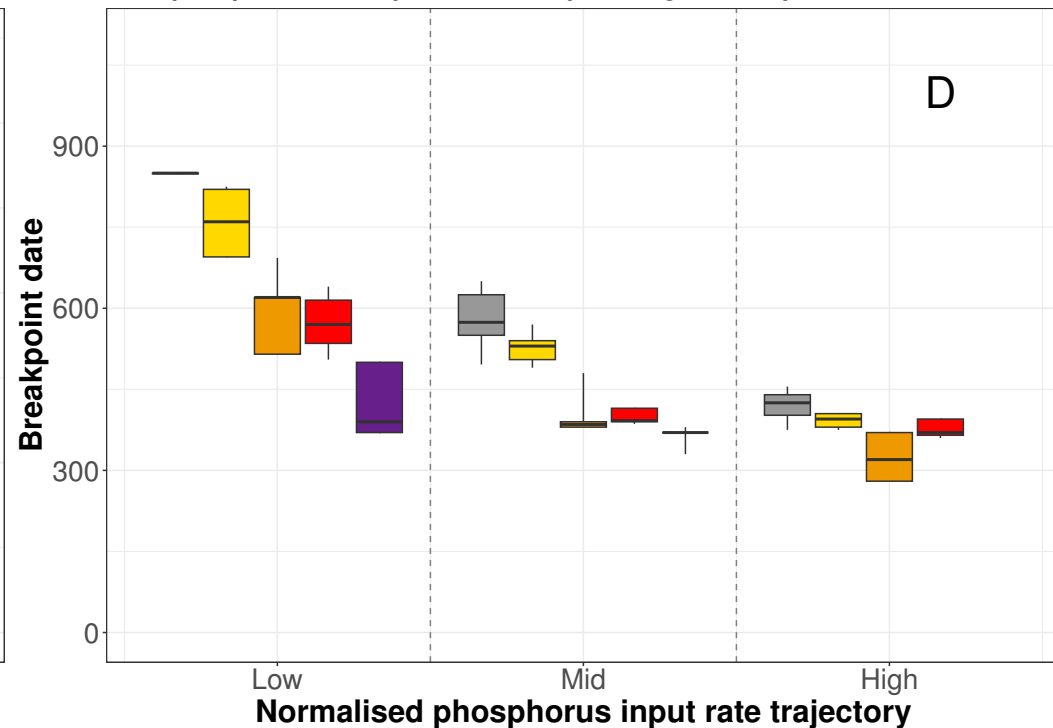
Easter Island: Multiple slow rates plus single uncoupled noise



TRIFFID: Multiple slow rates plus single uncoupled noise



Lake phosphorus: Multiple slow rates plus single uncoupled noise



Combination  Baseline  Low T, Low N  Low T, High N  High T, Low N  High T, High N